

Temperature advection derived from Doppler radar
wind profiles

Susanne Jonker

December 2003

Contents

Contents	3
Chapter 1 Introduction	5
2.1 Principles.....	7
2.2 Scan strategy	7
2.3 Method for wind profile retrieval.....	8
2.4 Availability	9
2.5 Quality.....	10
Chapter 3 Thermal wind and advection	13
3.1 Thermal wind	13
3.2 Temperature gradient	16
3.3 Advection.....	18
3.4 Potential use of advection calculated from radar wind profiles.....	20
Chapter 4 Data	23
4.1 Wind profiles	23
4.2 Verification data.....	23
4.2.1 HIRLAM data	23
4.2.2 Radiosonde data	23
4.3 Selection of cases	23
Chapter 5 Results	25
5.1 General features	25
5.2 September 10 th 2003, 12 UTC.....	25
5.2.1 Synoptic situation.....	25
5.2.2 Calculated temperature advection	27
5.2.3 Comparison radar-advection with Hirlam advection	28
5.3 May 5 th 2003, 6 UTC	31
5.3.1 Synoptic situation:.....	31
5.3.2 Calculated temperature advection	32
5.3.3 Comparison radar-advection with Hirlam advection	33
Chapter 6 Conclusions and recommendations	37
6.1 Conclusions.....	37
6.2 Recommendations.....	37
References.....	39
Appendix A Symbols and constants	41
Appendix B Influence of grid size on the calculated temperature gradient	43
Appendix C Program code used for advection calculation	45
C.1 Calculating temperature advection from Doppler radar wind profiles.....	45
C.2 Calculating temperature advection from Hirlam data	45

Chapter 1 Introduction

Doppler radars can be used in two different ways: as a conventional radar where the intensity of the received radio waves is measured and as a genuine Doppler radar where the mean radial velocity of the scattering particles is measured. The Royal Netherlands Meteorological Institute (KNMI) operates two Doppler radars which are (up till now) used to measure reflectivity (to determine rain rates), occurrence of hail and vertical wind profiles for forecasting and research purposes. This pilot study focuses on a new possible quantity that can be derived from radar data: *temperature advection*.

With Doppler radar, the advection can be calculated using the change of the geostrophic wind with height. In theory, profiles of temperature advection can be calculated up till the height where wind data are available. Knowledge about the present state of the atmosphere with regard to advection profiles may help forecasters to improve weather forecasts.

This report is the result of an exploratory study on the possibility to derive temperature advection from Doppler radar wind profiles and makes a first estimation of the quality of the results by comparing the calculated advection with model data. For this purpose, two case studies have been selected, on which days an intercomparison between the calculated and observed advection has been made.

Although many more questions did arise during our research, this report will give answers to the following questions:

- Is it possible to deduce temperature advection profiles from Doppler radar wind profiles?
- Do values for advection seem reasonable when compared to model output? If not, what are the possible reasons?
- In what way can profiles of temperature advection deduced from Doppler radar wind profiles be useful to weather forecasters?

The outline of this report is as follows:

In Chapter 2 the basic principles of radar technique will be discussed. The equations used and assumptions made for calculating the advection from both radar data and Hirlam data will be treated in Chapter 3. Next, we will shortly describe the data we used for our calculations and verification. In Chapter 5, we will treat the two cases we studied. First we will show the synoptic situation during the cases, after which we will compare the advection, calculated using radar data with the advection found using Hirlam data.

The conclusions of this pilot study and recommendation for further research will be given in Chapter 6.

We refer to Appendix A for the meaning of the symbols used and to Appendix C for information about the C code used to calculate the temperature advection from Doppler radar wind profiles and from Hirlam data.

Chapter 2 Doppler radar

2.1 Principles

Radar is an active remote sensing device: it transmits and receives radio electromagnetic waves. Part of these waves can be scattered back by particles (e.g. rain droplets) in the atmosphere. The radar measures how long it takes for a pulse to return, which gives information about distance of the scattering particles. From the amount of radiation that has returned the reflectivity can be determined, which is a function of size and number of scattering particles. This way radar can be used to estimate the precipitation intensity.

A Doppler radar can also determine the speed at which scattering particles move from or towards the radar. Only one component of the wind, the radial velocity, can be determined. This is done by measuring the rate of phase change. From the time it takes for the pulse of electromagnetic energy to travel to the target and back to the antenna, one can determine the distance of the particles from the radar. In combination with the known azimuth and elevation angle (see Figure 2.1), the position of the particles can be determined. Because there is a difference in speed between the targets and the radar (which is not moving), a phase difference between the transmitted and the received radiation can be observed. This is called the Doppler effect. When a phase shift of φ is measured, the wave has

travelled a distance of $\lambda \left(n + \frac{\varphi}{2\pi} \right)$, where λ is the wavelength and n is an unknown integer. The

distance between the radar and the particles is half that distance (the *range*): $x = \frac{\lambda}{2} \left(n + \frac{\varphi}{2\pi} \right)$. By

measuring the rate of phase change between two subsequent scattered pulses, the difference in

distance of the scattering particles can be determined: $\Delta x = \frac{\lambda}{2} \left(\frac{\Delta \varphi}{2\pi} \right)$. The velocity of the scattering

particles can be calculated by dividing the difference in distance by the time between the two pulses

(the pulse repetition time *PRT*): $v = \frac{\lambda}{PRT} \left(\frac{\Delta \varphi}{4\pi} \right)$. The maximum phase change that can be determined

is $-\pi < \varphi < \pi$, which implies that the radial velocity has a maximum unambiguous value as well. This maximum unambiguous velocity is given by:

$$v_{\max} = \frac{\lambda}{4PRT}$$

For the KNMI C-band Doppler radars, which emit radiation with a wavelength of 5.3 cm and use a PRT of 1 ms⁻¹, the maximum unambiguous velocity is approximately 13 ms⁻¹. It will be detailed below that this maximum velocity can be extended by a factor of 3.

2.2 Scan strategy

KNMI operates two identical C-band Doppler weather radars. One is stationed in Den Helder (52.96N, 4.79E), the other in De Bilt (52.10N, 5.18E). For this study, only wind profiles measured at De Bilt have been used.

The elevation is the angle between the direction of the radar beam and the horizon (see Figure 2.1). The azimuth is the clockwise horizontal direction of the radar beam expressed with respect to true north. Every sample of data retrieved at one particular azimuth is called a ray. Dedicated Doppler scans are repeated every 15 minutes and are performed at 10 different elevations (0.5°, 2°, 3.5°, 5.0°, 7.0°, 9.0°, 12°, 15°, 20°, and 25°). These 10 elevations have been optimized for profiling up to an altitude of about 6 km. At each elevation the radar scans 360 rays, the beam width being about 1 degree. In 15 seconds, the 360 degrees are covered, after which this is repeated at another elevation.

As is mentioned before, the maximum unambiguous velocity would normally be 13 ms^{-1} when a *PRF* of 1 ms is used. With the so-called dual *PRF* technique however, the maximum unambiguous velocity can be increased. This technique uses two different *PRF*'s in the velocity measurement. A high and a low *PRF* are used to obtain two different velocity measurements that may or may not be folded outside their unambiguous velocity intervals. From their difference it can be inferred how many times the velocities are folded, so that the measured velocity can be unfolded. An extensive analysis and a technique for correction of dual-*PRF* velocity data are presented by Holleman and Beekhuis (2003). The dual-*PRF* technique increases the maximum unambiguous velocity to 39.9 ms^{-1} .

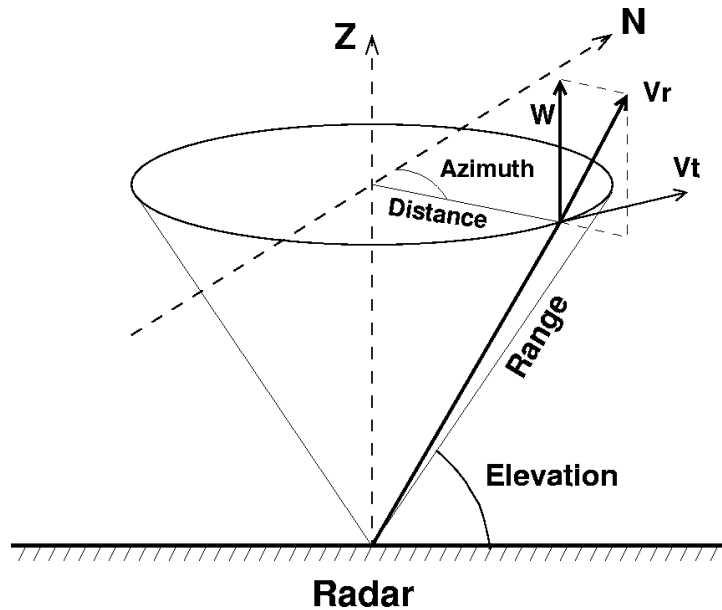


Figure 2.1 Schematic overview of the radar geometry used to measure Doppler wind profiles. The range, azimuth and elevation, which are the scanning directions of a weather radar, are indicated. The radial velocity V_r , the tangential velocity V_t , and the vertical velocity w components of the local wind files are shown (Figure taken from Holleman, 2003)

2.3 Method for wind profile retrieval

There are several techniques to deduce the upper air wind data from Doppler radar observations. One of those techniques is the Velocity Azimuth Display (VAD) technique. When the mean radial velocity at constant range and elevation is displayed as a function of azimuth, the resulting curve will have the form of a sine (see Figure 2.2 for an example). The wind speed can be determined from the amplitude, and the direction can be derived from the phase of the sine. A function is fitted to the observed VAD to obtain these quantities. One disadvantage of the VAD retrieval method is that the conversion of a Doppler volume scan to a wind profile is not straightforward. A large series of VAD's of each height layer needs to be processed to obtain wind profile.

At the KNMI, a Volume Velocity Processing (VVP) method is used to obtain wind profiles. The main advantage of this method is that all available data of the scanned volume is processed at once (instead of combining the results of several VAD's as is done with the VAD method). This means that a multi-dimensional linear fit of the radial velocity equation (where the velocity is a function of azimuth, elevation and range) to the observed Doppler volume data. As a measure of quantity of the fit, the standard deviation of the fit is calculated too.

At the KNMI, wind profiles are calculated from the mean radial velocity data using the Rainbow VVP module. This commercial implementation of the VVP retrieval method was delivered with the KNMI Doppler radars.

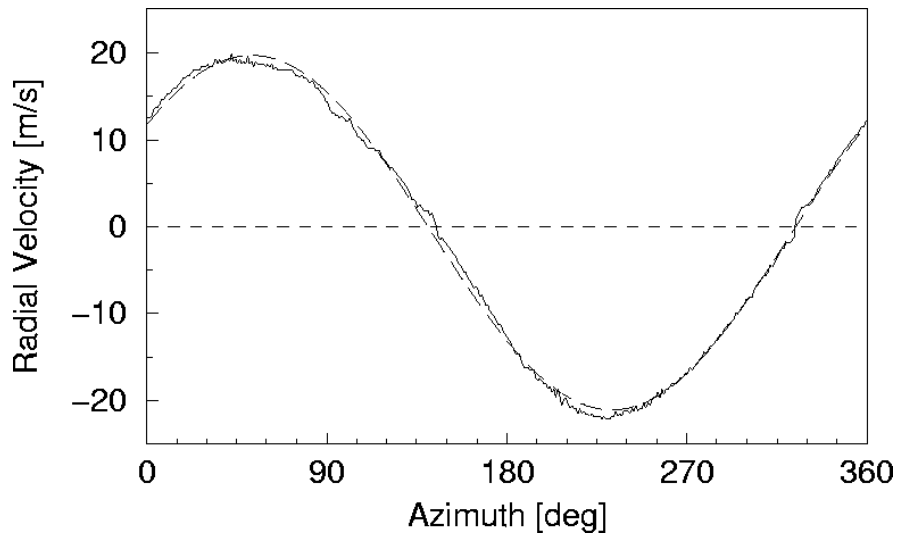


Figure 2.2 Example of a Velocity Azimuth Display (VAD) obtained from a volume measurement. The long-dashed curve shows a sine fit through the observed VAD. Maximum wind speed is 20.4 ms^{-1} and 217 degrees.

2.4 Availability

In theory, not only the movement of precipitation and clouds can be detected, the motion of clear air may also be tracked because there is some backscattering of the radar signal from regions where there is a sharp index-of-refractions gradient, owing to temperature and moistures inhomogenities. This would imply that wind profiles could be observed using Doppler radar, even when precipitation is not taking place.

In practice, we see that the total number of available wind factors is decreasing with increasing height, while the mean wind speed is increasing with increasing height (see Figure 2.3).

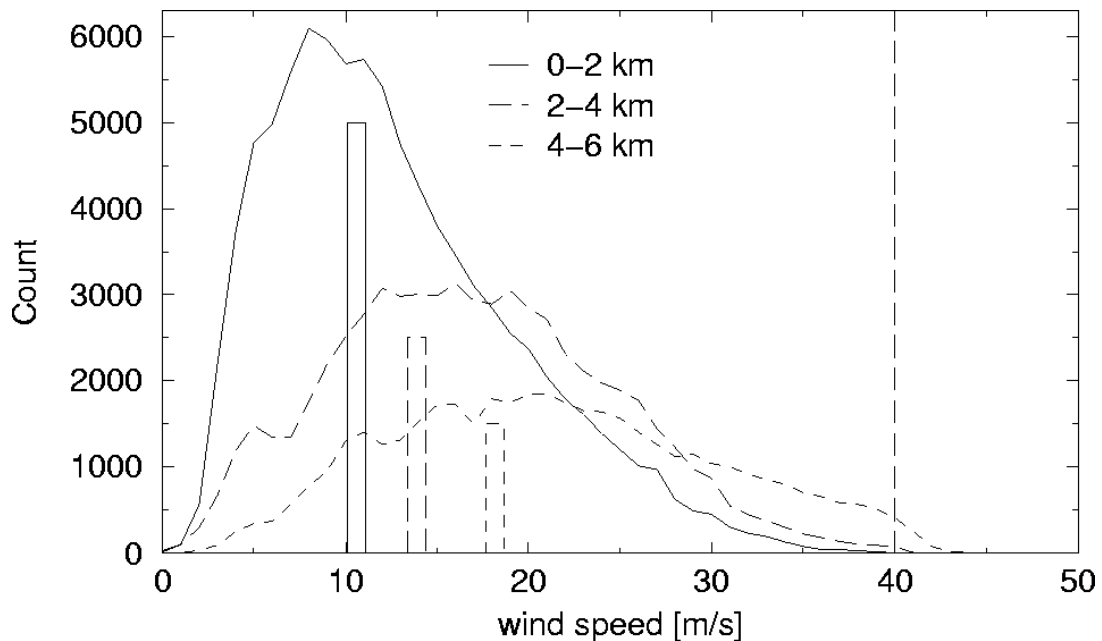


Figure 2.3 Histogram of the observed wind speeds for three different height layers and using wind speed bins of 1 ms^{-1} . The wind speeds are obtained from the radar using the retrieval method (VVP1) very similar to the one used at De Bilt (which is VVP Rainbow). A standard deviation threshold of 2 ms^{-1} is applied. The vertical bars represent the mean wind speeds as obtained from the radiosonde observations over the same period. Total number of wind vectors is 226100 per layer. Figure taken from Holleman, 2003.

In the boundary layer insects, birds, dust and the aforementioned refractive-index gradients may also be seen as particles moving along the wind. Above the boundary layer the radiation will be scattered by precipitation only. Holleman (2003) confirmed this, as is shown in Table 2.1. Table 2.1 lists for 1 km height ranges the fraction of the number of available wind vectors to the maximum number of vectors. This availability fraction decreases from 0.39 in the lowest height range to 0.162 in the highest height range. The latter corresponds very well with the observed precipitation occurrence of 0.141 (Holleman, 2003).

Table 2.1 Quantitative results of the histogram analysis for 1 km height ranges, according to Holleman (2003)

Height	Availability
0-1 km	0.393
1-2 km	0.409
2-3 km	0.303
3-4 km	0.248
4-5 km	0.213
5-6 km	0.162

2.5 Quality

The Doppler radar wind profiles have been verified against the profiles from the collocated radiosonde station by Holleman (2003). For this, pairs of wind vectors from the radar and radiosonde with matching time and height coordinates are collected. This collection of wind vector pairs has been used to calculate verification parameters like root-mean-square error, bias and the standard deviation of the wind speed.

When choosing a threshold on the allowed standard deviation a balance has to be found between the quality of the wind vectors and their availability. Holleman (2003) found an optimum when applying a standard deviation of 2 ms^{-1} .

The bias and standard deviation profiles obtained from the verifications of the Rainbow VVP module against the radiosonde observations are shown in Figure 2.4 (Holleman, 2003).

Both the bias for speed and direction of the wind vectors are negative below 1 km. Above that height the wind speed bias is generally smaller than 0.5 ms^{-1} and positive, indicating that radar wind speeds are slightly higher than those of the radiosonde. The wind speed bias is much smaller than the corresponding standard deviation, and it is therefore considered to be within acceptable limits.

The required accuracy of upper air wind speed measurements is 1 ms^{-1} according to the WMO guide on Meteorological Instruments and Methods of Observations. This confirms that the observed wind speed bias is within acceptable limits and it suggests that the observed standard deviation, which is deduced from a comparison between two measurements, just satisfies the accuracy requirements.

The wind direction bias shows a remarkable sign change between 3 and 4 km altitude. According to Holleman (2003), this sign change is not observed in the wind direction bias as a function of wind speed and therefore must originate from some unexplained height effect. The standard deviation of the wind direction is decreasing with increasing height. From other analyses Holleman (2003) concluded that for wind speeds above 10 ms^{-1} the Doppler radar is capable of providing wind profiles that satisfy the stringent accuracy (standard deviation) requirements by WMO.

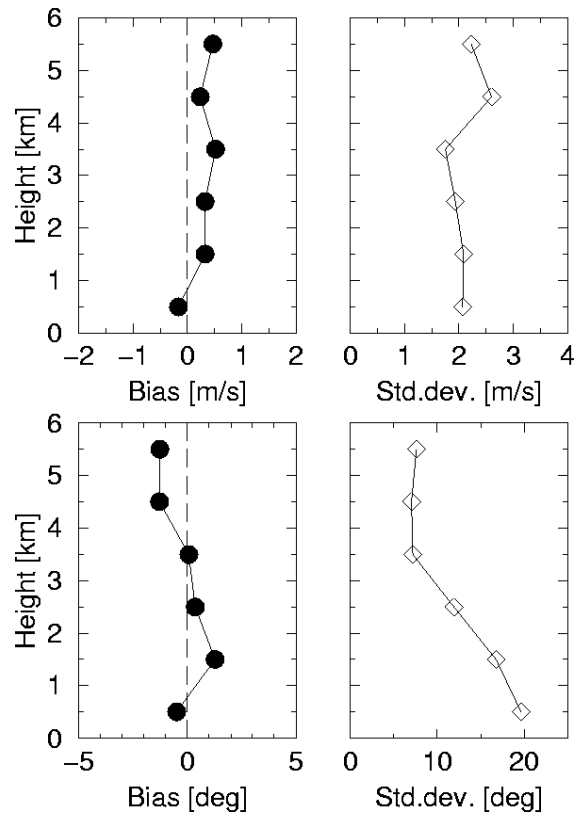


Figure 2.4 Profiles of bias and standard deviation of the wind speed and direction as obtained from verification of Rainbow VVP modules against radiosonde.

For more information on the Doppler radars of the KNMI, its setting, the method of wind profile retrieval techniques and performance we refer to Holleman (2003).

In the next chapter we will show how wind profiles obtained using Doppler radar can be used to calculate temperature advection.

Chapter 3 Thermal wind and advection

The main goal of this study is to deduce values for temperature advection from wind profiles observed with Doppler radar. In this chapter will be shown how this can be done. It will also be detailed how we calculated the advection using Hirlam data. Both advectons will be compared in Chapter 5.

The temperature advection will be calculated using the following equation (see section 3.3):

$$\frac{\partial T}{\partial t}_{adv} = -\left(u \frac{\partial T}{\partial x} + v \frac{\partial T}{\partial y}\right)$$

To calculate the temperature advection, velocities u and v are needed, and temperature gradients $\partial T/\partial x$ and $\partial T/\partial y$. The wind vectors are observed with the Doppler radar, and we will approximate the temperature gradients using the thermal wind equation.

Basic theory and equations of the thermal wind will be elaborated in section 3.1. As we will see, assumptions about the temperature profile in the lower atmosphere need to be made when deriving the advection from the observed wind profiles. Backgrounds on these assumptions will be discussed in section 3.2. Section 3.3 deals with the equations used to calculate the advection, using Doppler radar data, “vertical” Hirlam data and “horizontal” Hirlam data.

In section 3.4 will be described in what way observed temperature advection profiles can provide valuable information about rotation, temperature tendency, timing of front passages and development of the height field and/or vertical motions. Advection observations may therefore be useful for forecasters.

3.1 Thermal wind

For midlatitude synoptic scale disturbances the Coriolis force and the pressure gradient are in approximate balance. Retaining only these two terms in the equations of motion we obtain as a first approximation the geostrophic relationship (Holton, 1979):

$$v_g \approx \frac{1}{f\rho} \frac{\partial p}{\partial x} \quad \text{and} \quad u_g \approx -\frac{1}{f\rho} \frac{\partial p}{\partial y} \quad (3.1)$$

where v_g is the y -component of the geostrophic wind, u_g is the x -component of the geostrophic wind, p is the pressure, ρ is the density and $f \equiv 2\Omega \sin \varphi$ is called the Coriolis parameter. Here Ω is the angular speed of rotation of the earth and φ is the latitude. When assuming that the observed wind is geostrophic, we imply the following:

- there is no friction
- it is a stationary situation
- isohypses are straight (no curve)
- no vertical advection is taking place

According to Stull (2000), most of the atmosphere is nearly in geostrophic equilibrium, so we assume that the geostrophic wind can be given by the observed wind.

This geostrophic wind must have vertical shear in the presence of a horizontal temperature gradient, as can be shown from simple physical considerations based on hydrostatic equilibrium.

Because the geostrophic wind is proportional to the horizontal pressure gradient, we see that for the case shown in Figure 3.1 there is a geostrophic wind directed along the y -axis, which increases in magnitude with height as the slope of the isobars increases. From the hydrostatic equation it can be shown that the height increment δz corresponding to a given pressure increment δp is given by

$$\delta z \approx -\frac{\delta p}{p} \frac{RT}{g} \quad (3.2)$$

where R is the gas constant for dry air, T is the temperature and g is the gravitational acceleration. This equation can be derived from combining the hydrostatic equilibrium $\frac{dp}{dz} = -\rho g$ and the ideal gas law $p = \rho RT \Rightarrow \rho = \frac{p}{RT}$. The hydrostatic equilibrium is an excellent approximation for the vertical dependence of the pressure field in the real atmosphere. Only for intense small-scale systems such as squall lines and tornadoes it is necessary to consider departures from hydrostatic balance (Holton, 1979).

Equation (3.2) means that in Figure 3.1, $T_{x2} > T_{x1}$ because $(\delta z)_{x1} < (\delta z)_{x2}$. Thus, the increase with height of the positive x -directed pressure gradient must be associated with a positive x -directed temperature gradient. The air in a vertical column at x_2 must occupy a greater depth for a given pressure drop (because it is warmer and less dense) than the air at x_1 .

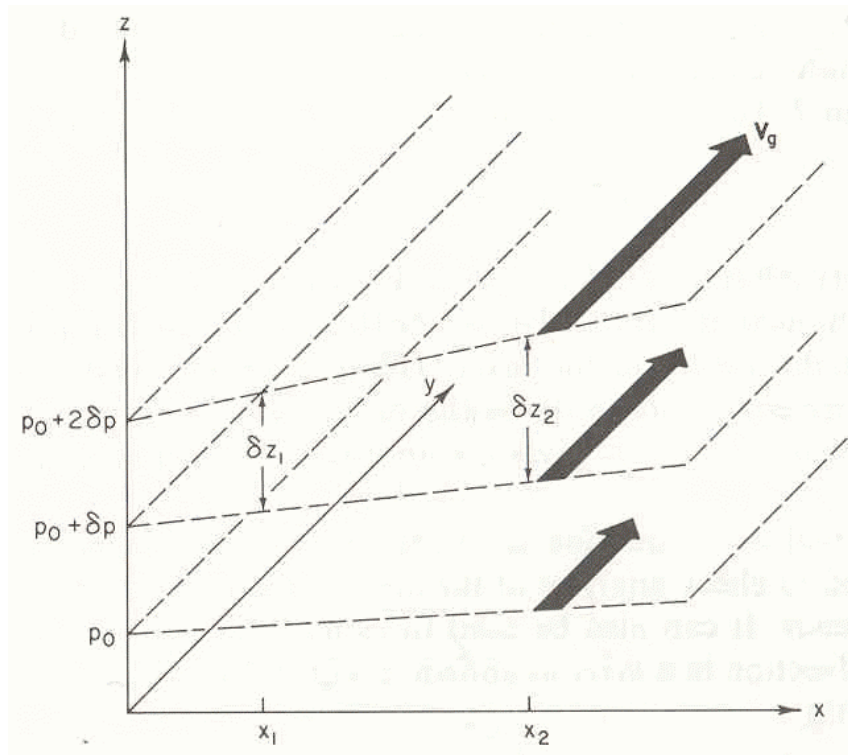


Figure 3.1 Relationship between vertical shear of the geostrophic wind and horizontal temperature gradients (After Holton, 1979)

The equations for the rate of change of the geostrophic wind components with height are most easily derived using the isobaric coordinate system. The geostrophic wind components in isobaric coordinates are:

$$v_g = \frac{1}{f} \frac{\partial \Phi}{\partial x} \quad \text{and} \quad u_g = -\frac{1}{f} \frac{\partial \Phi}{\partial y} \quad (3.3)$$

where Φ is the geopotential $\left(\Phi \equiv \int_0^z g dz \right)$ and where the derivatives are evaluated with the pressure held constant. Rewriting the hydrostatic equation with the ideal gas law gives:

$$\frac{\partial \Phi}{\partial p} = \frac{g \partial z}{\partial p} = -\frac{1}{\rho} = -\frac{RT}{p} \quad (3.4)$$

Differentiating (3.3) with respect to pressure and applying (3.4) we obtain:

$$\begin{aligned} \frac{\partial v_g}{\partial p} &= \frac{1}{f} \frac{\partial}{\partial x} \left(\frac{\partial \Phi}{\partial p} \right) \Rightarrow \frac{\partial v_g}{\partial p} = -\frac{1}{f} \frac{\partial}{\partial x} \left(\frac{RT}{p} \right) \Rightarrow p \frac{\partial v_g}{\partial p} = -\frac{R}{f} \left(\frac{\partial T}{\partial x} \right)_p \Rightarrow \\ \frac{\partial v_g}{\partial \ln p} &= -\frac{R}{f} \left(\frac{\partial T}{\partial x} \right)_p \end{aligned} \quad (3.5)$$

Integrating from pressure level p_1 to p_2 ($p_2 < p_1$) gives

$$\int_{p_1}^{p_2} dv_g = - \int_{\ln p_1}^{\ln p_2} \frac{R}{f} \left(\frac{\partial T}{\partial x} \right)_p d \ln p \Rightarrow v_{g(p_2)} - v_{g(p_1)} = -\frac{R}{f} \left(\frac{\partial \langle T \rangle}{\partial x} \right)_p (\ln p_2 - \ln p_1)$$

which results in the following equation for the y -component of the *thermal wind*:

$$v_T = v_{g(p_2)} - v_{g(p_1)} = -\frac{R}{f} \left(\frac{\partial \langle T \rangle}{\partial x} \right)_p \ln \left(\frac{p_2}{p_1} \right) \quad (3.6)$$

where $\langle T \rangle$ denotes the mean temperature in the layer between pressure p_2 and p_1 .

For the u -component of the thermal wind a similar derivation gives:

$$u_T = u_{g(p_2)} - u_{g(p_1)} = \frac{R}{f} \left(\frac{\partial \langle T \rangle}{\partial y} \right)_p \ln \left(\frac{p_2}{p_1} \right) \quad (3.7)$$

The thermal wind blows parallel to the isotherms with the warm air to the right facing downstream in the northern hemisphere. As illustrated in Figure 3.2, a geostrophic wind which turns counter clockwise with height (backs) is associated with cold-air advection. Conversely, clockwise turning (veering) of the geostrophic wind implies warm advection by the geostrophic wind in the layer. It is therefore possible to get a reasonable estimate of the horizontal temperature advection and its vertical dependence at a given location solely from data on the vertical profile of the wind given by a single sounding.

To derive the temperature gradient from equations (3.6) and (3.7), we need values for $\ln(p_2/p_1)$. When calculating advection using only Doppler radar data, we do not have these values (we only have values for the measuring heights). How we obtain these values will be discussed in the next section. For our verification in Chapter 5 we will use Hirlam data. Because all variables of eq. (3.6) and (3.7) are available in the model, no extra assumptions need to be made. Section 3.3 deals with the calculation of the advection.

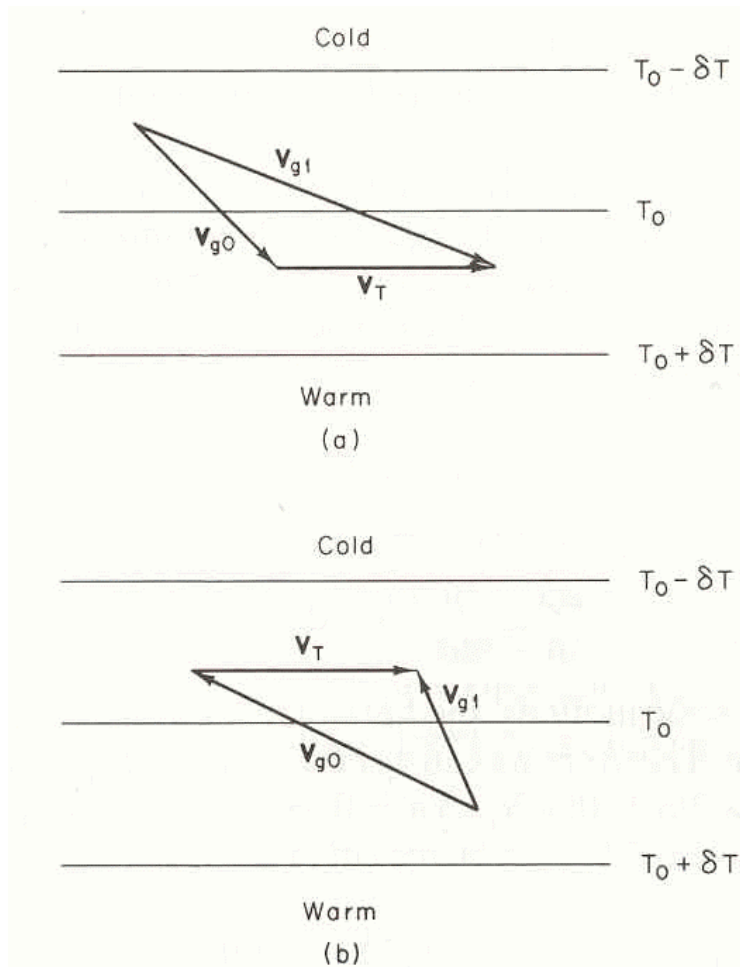


Figure 3.2 The relationship between turning of the geostrophic wind and temperature advection: (a) backing of the wind with height; (b) veering of the wind with height (After Holton, 1979).

3.2 Temperature gradient

To calculate the advection we need the temperature gradient. As became clear in the previous section (equations (3.6) and (3.7)), additional data about the pressure profile is needed to deduce this temperature gradient from the thermal wind.

Because we do not have information about pressure, but we *do* have information about the measuring heights (wind profile measurements are performed every 200 m) we have to approximate the pressure profile using an estimate for the mean temperature in the different layers of the troposphere. We will do this using the *hypsometric equation*, of which the derivation is shown below.

We start with the hydrostatic equation:

$$\frac{dp}{dz} = -\rho g \quad (3.8)$$

and the ideal gas law:

$$P = \rho RT \Rightarrow \rho = \frac{P}{RT} \quad (3.9)$$

Substituting 3.9 in 3.8 gives:

$$\frac{dp}{dz} = -\frac{pg}{RT} \Rightarrow \frac{dp}{p} = -\frac{g}{RT} dz \quad (3.10)$$

Integration yields:

$$\int_{p_1}^{p_2} \frac{1}{p} dp = -\frac{g}{R} \int_{z_1}^{z_2} \frac{1}{T} dz \quad (3.11)$$

This integral can only be solved when we know how T changes with height, or when we determine the mean temperature over the layer between z_2 and z_1 . In case of the latter, the formula becomes:

$$\int_{p_1}^{p_2} d \ln p = -\frac{g}{R} \left(\overline{\frac{1}{T}} \right) \int_{z_1}^{z_2} dz$$

$$\ln \left(\frac{p_2}{p_1} \right) = -\frac{g}{R} \left(\overline{\frac{1}{T}} \right) (z_2 - z_1) \quad (3.12)$$

Recalling that $\ln(x) = -\ln(1/x)$ and approximating $T \approx 1/\overline{(1/T)}$ one gets the *hypsometric equation*:

$$(z_2 - z_1) = \frac{R}{g} \overline{T} \ln \left(\frac{p_1}{p_2} \right) \quad (3.13)$$

As can be seen from this relation, a ten percent error in the mean temperature ($\approx 30\text{K}$) produces an error of approximately 10 percent in $\ln(p_1/p_2)$. The error becomes larger when temperatures are dropping. A ten percent error is tolerable for our purposes. Therefore we concluded that we can use the “1976 U.S. Standard Atmosphere” (Stull, 2000) to estimate reasonable values for temperature and pressure at different heights. For that idealized, dry, steady state approximation of the atmospheric state as a function of height the following equation is valid for the lower 11km:

$$T = 288.15 - (6.5\text{K/km}) \cdot H \quad (3.14)$$

where H is the geopotential height ($H \equiv \frac{\Phi(z)}{g_0}$, where g_0 is the global average of gravity at mean sea

level). H is numerically almost identical to the geometric height (Stull, 2000). This means we work with a constant lapse rate of 6.5 K/km and a T_0 of 288.15 K.

This last equation gives \overline{T} , which will be used in equation 3.13 to calculate $\ln(p_1/p_2)$. This will serve as input for equations (3.6) and (3.7), which equations we use to calculate $\frac{\partial \langle T \rangle}{\partial x}$ and $\frac{\partial \langle T \rangle}{\partial y}$.

We then get:

$$\frac{\partial \langle T \rangle}{\partial x} = \frac{f}{g} \frac{v_{g(p2)} - v_{g(p1)}}{z_2 - z_1} \left[T_0 - 6.5 \left(\frac{z_1 + z_2}{2} \right) \right] \quad (3.15)$$

$$\frac{\partial \langle T \rangle}{\partial y} = -\frac{f}{g} \frac{u_{g(p2)} - u_{g(p1)}}{z_2 - z_1} \left[T_0 - 6.5 \left(\frac{z_1 + z_2}{2} \right) \right] \quad (3.16)$$

3.3 Advection

Advection is given by $\frac{\partial T}{\partial t}_{adv} = -\vec{v} \cdot \nabla T$. The two horizontal components are

$$\frac{\partial T}{\partial t}_{adv} = -\left(u \frac{\partial T}{\partial x} + v \frac{\partial T}{\partial y}\right) \quad (3.17)$$

The advection can be calculated by using either of the two winds used to calculate the thermal wind: both the upper and the lower wind will give the same result. This can be shown by rewriting into

$\frac{\partial T}{\partial t}_{adv} = -\vec{v} \cdot \nabla T$ into $\frac{\partial T}{\partial t} = |\vec{v}_2| |\nabla T| \cos(\alpha) = |\vec{v}_1| |\nabla T| \cos(\beta)$, which can be illustrated by Figure 3.3:

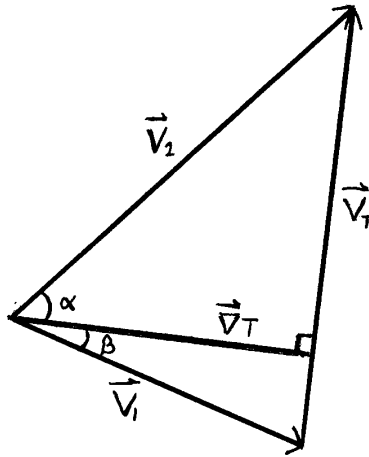


Figure 3.3 Illustration of advection calculation where v_1 is the wind at level 1, v_2 is the wind at level 2, v_T is the thermal wind, ∇T is the gradient in temperature

As can be seen from this figure, the perpendicular component of the wind to the temperature gradient (which is the advecting wind) is the same for both winds.

Because the gradients in temperature are valid for height in between the height at which wind velocities are determined, we will average the advection by both winds. See Figure 3.4 for visualisation.

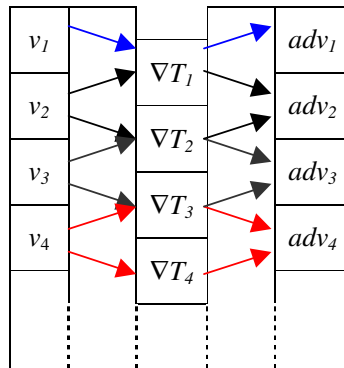


Figure 3.4 Calculation of advection using wind profile data from the Doppler radar or Hirlam

This “vertical method” for calculating the advection (i.e. the gradient of temperature is estimated using information about the vertical distribution of velocities) was used for calculating both advection from observed velocities (from the Doppler radar) and velocities from the Hirlam model. For the Doppler radar calculations, assumptions have been made about the temperature (and thus pressure) profile by using the standard atmosphere. When using Hirlam data, the temperatures and pressures of the model have been used.

A “horizontal method” for calculating the advection has also been used for estimation of advection using Hirlam data. This will shortly be described hereafter.

A grid of 1x1 degree around De Bilt has been defined (Figure 3.5). The data from the model have been interpolated to those grid points. In Appendix B is shown that the interpolation distance does not have a great influence on the outcome.

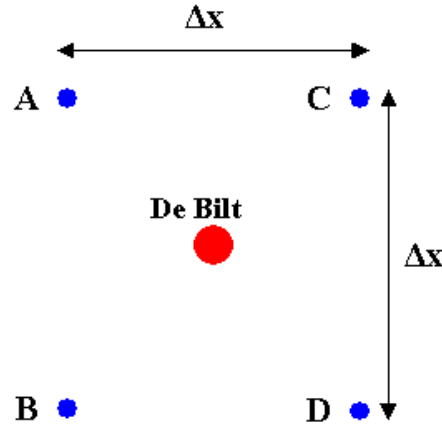


Figure 3.5 Grid around De Bilt used for advection calculation from Hirlam data using the “horizontal method”

The temperature gradient in the x -direction at the location of De Bilt has been approximated by (see Figure 3.5):

$$\frac{dT}{dx} = \frac{(T_C + T_D) - (T_A + T_B)}{\Delta x} \text{ with } \Delta x = 2 \text{ degrees} \approx 68.45 \text{ km}$$

The u -wind at De Bilt has been approximated averaging the four u -winds of the grid.

The temperature gradient in the y -direction at the location of De Bilt has been approximated by (see Figure 3.5):

$$\frac{dT}{dy} = \frac{(T_A + T_C) - (T_B + T_D)}{\Delta x} \text{ with } \Delta x = 2 \text{ degrees} \approx 111.18 \text{ km}$$

The v -wind at De Bilt has been approximated averaging the four v -winds of the grid.

With these “ingredients” we used eq. (3.17) to calculate the temperature advection with the “horizontal method”.

Summarizing, horizontal temperature advection will be calculated in three different ways:

- 1) horizontal temperature advection derived from Doppler radar wind profiles using the thermal wind equation (this will hereafter be referred to as “Radar advection”)
- 2) horizontal temperature advection derived from Hirlam wind profiles using the thermal wind equation (this will hereafter be referred to as “Hirlam vertical advection”)
- 3) horizontal temperature advection derived from horizontal temperature distribution data (this will hereafter be referred to as “Hirlam horizontal advection”).

3.4 Potential use of advection calculated from radar wind profiles

In this section we try to gain insight in how forecasters can benefit from the availability of profiles of temperature advection deduced from radar data.

Geostrophy

Looking at the assumptions made when deducing temperature advection from Doppler radar wind profiles it is obvious that the calculated advection will not give reliable outcomes when applied in situations that are far from geostrophy, like intense small-scale systems. Calculating the Rossby number could give an impression of the size of the non-geostrophic wind components in the observed wind.

Rotation

Figures of temperature advection are a good way to show the rotation of the wind field with height. Next to change of wind speed with height (shear), rotation with height is often an important variable for the development of systems in the atmosphere. Displaying calculated temperature advection like we will do in this report emphasises the rotation in the wind field, which would go unnoticed when examining just the wind profiles.

Temperature tendency

Advection data can give information on the temperature tendency. This however, is only a very rough estimate, because the temperature tendency is influenced by another two terms, according to the following equation (Bluestein, 1992):

$$\frac{\partial T}{\partial t} = -\vec{v} \cdot \vec{\nabla}_p T + \omega \sigma \frac{p}{R} + \frac{1}{C_p} \frac{dQ}{dt} \quad (3.18)$$

where T is the temperature, t is the time, \vec{v} is the wind, ω is the vertical velocity in pressure coordinates ($\omega = dp/dt$), σ is a measure of the static stability, p is the pressure, R is the gas constant, C_p is the specific heat at constant pressure and dQ is heat added or removed from the air parcel. The first term on the left hand side (LHS) is the quasi-horizontal temperature advection, the second term is the adiabatic temperature change associated with the work done on of by the air parcel by the environment during vertical displacements. The 3rd term on the LHS is the diabatic heating. With our calculations of the temperature advection we only estimate the first term on the LHS. We should keep in mind that the advection is not the only term influencing the temperature tendency. In practice, the rule-of-thumb is used that the observed temperature tendency is half the advection.

Vertical motions

For the thermal advection the following applies:

$$\omega_{TA} \propto -\frac{R}{\sigma p} \left(-\vec{v}_g \cdot \vec{\nabla}_p T \right), \quad (3.19)$$

where ω_{TA} is the vertical velocity in pressure coordinates caused by temperature advection ($\omega = dp/dt$), R is the gas constant, σ is a measure of the static stability, p is the pressure, \vec{v}_g is the geostrophic wind and T is the temperature.

This equation is deduced from the quasi-geostrophic ω equation found in books on dynamic meteorology (e.g. Bluestein (1992) and Holton (1979))

This means that warm advection (WA) is associated with ascent, and cold advection (CA) is associated with descent. Forecasters may use figures showing maxima and minima of temperature advectons to draw conclusions about vertical motions. They should keep in mind thought, that other

terms in the quasi-geostrophic ω equation also affect the observed vertical velocity (e.g. vorticity advection and differential vorticity advection and diabatic heating).

Differential temperature advection

Besides the quasi-geostrophic ω equation, another equation can be derived by combining the vorticity and thermodynamic equations: the prognostic equation for height tendency χ ($\chi \equiv \frac{\partial \Phi}{\partial t}$; Bluestein, 1992). In this equation we find a term indicating the differential warm advection with height:

$$\chi \propto \frac{f_0}{\sigma} \frac{\partial}{\partial p} \left[-v_g \cdot \nabla \left(-\frac{\partial \Phi}{\partial p} \right) \right] \tag{3.20}$$

Because temperature T of a layer is proportional to the thickness of the layer ($T = -\frac{p}{R} \frac{\partial \Phi}{\partial p}$), the RHS

term in equation 3.20 is proportional to the vertical derivative of temperature advection. The effects of differential thermal advection can be thought of as follows. Typically, thermal advection is very small in the upper troposphere (above 500 mb), so it is really the low level advection that determines the 500 mb geopotential tendency. Cold advection in the lower levels will decrease the thickness of the 1000 -500 mb layer, and lower the heights at 500 mb, as would be expected (since cold advection decreasing with height is the same as warm advection increasing with height). Warm advection in the lower levels will increase the thickness of the 1000 -500 mb layer, and result in height rises at 500 mb [URL1].

Nowcasting

Especially nowcasting might benefit from information about temperature advection derived from Doppler radar wind profiles. A real time display on the Intranet could give nowcasters information on the timing of the passing of frontal systems in the atmosphere. Profiles of both Den Helder and De Bilt could be combined to give more information on the position of frontal zones.

This should be accompanied by an effort to increase knowledge on how the observed temperature can be interpreted and used for nowcasting.

Chapter 4 Data

4.1 Wind profiles

For the calculation of the thermal wind and temperature advection, wind profiles obtained with the Doppler radar in the Bilt (52.10°N, 5.17°E) have been used. For all available wind profiles in 2003 up till half October, profiles of advection have been calculated (up till 6 km). Two cases have been selected (see section 4.3). Wind data were only taken into consideration if the standard deviation was smaller than 2 ms^{-1} . For more information on radar data, see Chapter 2. More information on how advection was derived from wind profiles can be found in Chapter 3.

At the KNMI, radar data are stored in HDF-5 files. HDF stands for Hierarchical Data Format. This file format is developed by the National Center for Supercomputing Application (NSCA, URL2). The main advantages of this file format are that data and meta-data are stored in the same file, that the format is very flexible (new images can easily be added) and that the software libraries are public. The version that is currently used at the KNMI is KNMI-HDF5 version 3.4. For more information see URL3.

4.2 Verification data

4.2.1 HIRLAM data

For the verification of the radar-deduced temperature advection we mainly used data from the Hirlam model. Hirlam stands for High Resolution Limited Area Model and is a numerical short-range weather forecasting model operated by several national weather institutes throughout Europe. The model analyzes the state of the atmosphere 8 times a day, and makes 48-h forecasts 4 times a day. For our purposes we used Hirlam-22 data. We used this model because it has the highest availability. The horizontal resolution of the model is 22 km with 31 vertical levels.

For the advection calculations the initialized analyses (+0 “forecasts”) have been used. These were used because these are easier to access than the real analyses. Data were interpolated to De Bilt. With Hirlam data the advection was calculated using both wind profiles (referred to as the “vertical method”) and horizontal temperature distribution (referred to as the “horizontal method”).

4.2.2 Radiosonde data

For one of the cases we also tried to compare the advection data with the temperature change in time over the first 6km deduced from radiosondes data. This is only a very rough estimate, because the temperature tendency is influenced by another two terms (see eq. 3.18). With our calculations of the temperature advection we only estimate the first term on the LHS of that equation.

4.3 Selection of cases

The two main selection criteria for the cases were that

- 1) advection data were available (see Chapter 2 for more information on availability of wind data and thus advection data)
- 2) advection results should insinuate that some activity was taking place in the atmosphere (e.g. the passage of a front, storm or squall line)

The first case we selected is May 5th, 2003, 6UTC and is characterized by a large gradient in calculated advection, and a wide range of values (approx. -3.2 to 3.8 Kh^{-1} ; see Figure 5.13). Wind profiles suggest cold advection up till 3km, above which height warm advection is calculated.

We wanted the second case to be different from the first, so we could get a first impression on the influence of the meteorological situation on the results. During the second case (September 10th, 2003,

12 UTC) warm advection is derived from the wind profiles throughout the layer of 6 km deep (ranging from -0.4 to 3.0 K h^{-1}).

The synoptic situation and verification of the advection calculations of both cases will be presented in Chapter 5.

Chapter 5 Results

In this chapter we will first discuss a few general characteristics that struck us when first examining the figures of the calculated temperature advection. After that, we will take a close look at two cases: the first is September 10th 2003, 12 UTC and the second is May 5th 2003, 6UTC. We will start with a description of the synoptic situation, followed by presenting the calculated temperature advection from Doppler radar wind profile data. Next, we will compare our results with (radiosonde and) Hirlam data. See Chapter 3 for the equations used and Chapter 4 for a description of the data used.

5.1 General features

Figures of temperature advection calculated from the observed thermal wind look fairly consistent. Easily structures can be detected. We notice that the signal does not show much noise, even without applying any filtering method.

Figures of temperature advection are fairly good indicators of “activity in the atmosphere”. Without much effort situations like passage of fronts could be detected. This is however not totally attributable to the temperature advection, but also results from the fact that radar data have a higher availability when precipitation is taking place.

In some cases, the calculated values for temperature advection seem rather large (advection of over 10 Kh^{-1} and -10Kh^{-1} have been found). These values may not be realistic, especially when these advectons persist for several hours.

In the boundary layer *friction* is an important factor to take into account. The assumption of geostrophic balance is not valid here. This means that advection values below 1 km (during the day) or several hundreds of meter (during the night) might be biased towards warm advection. This is because friction causes a backing of the wind compared to the geostrophic wind. This was confirmed by most of the figures made.

5.2 September 10th 2003, 12 UTC

5.2.1 Synoptic situation

We will describe the synoptic situation using the surface analyses of Hirlam and the corresponding SATREP map for 12 UTC.

The surface analysis (Figure 5.1) shows a small, active low-pressure area north of Scotland that is moving in a northwesterly direction.

An upper level low (ULL) with a cold core (approx. $-25 \text{ }^\circ\text{C}$) is situated across the northern North Sea (Figure 5.2) is accompanied by an upper trough arcing to the SSE (this was more visible on the map of 6 hours before, not shown here). This system is moving to the east. To the south west of this band we find an upper warm front (Figure 5.1). A frontal system above the United Kingdom is approaching from the west.

Two jet streaks are situated to the west of the upper trough (indicated in purple). North of the easterly jet streak (in the upper trough) comma clouds with enhanced cumuli (EC) are positioned. The comma clouds indicate instability caused by the cold ULL and produce showers with lightning north east of the Netherlands. The second jet streak, belonging to the frontal system positioned above the United Kingdom, is moving eastward. Close to the left exit of this jet streak a low pressure area is formed, that is positioned above the southern North Sea (Figure 5.1)

Due to warm advection at high levels accompanying the frontal zone, intensity of the showers close to that zone decreases. While the warm front in the west is closing in on the upper trough, heavy rains are observed preceding the frontal system (Figure 5.3)

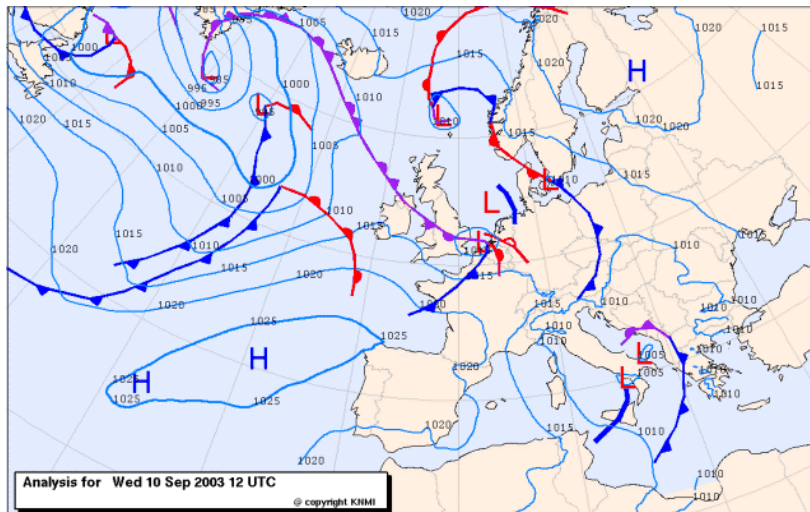


Figure 5.1 Synoptic situation on September 10th 2003, 12 UTC. Source: KNMI

The cold front is characterized as a cold front in warm advection (CF in WA). This is confirmed by Figure 5.4, where we observe warm advection in the position of the cold front. This warm advection is accompanying the frontal system approaching from the Atlantic Ocean and causes frontolysis to take place. This means that the cold front is not very active.

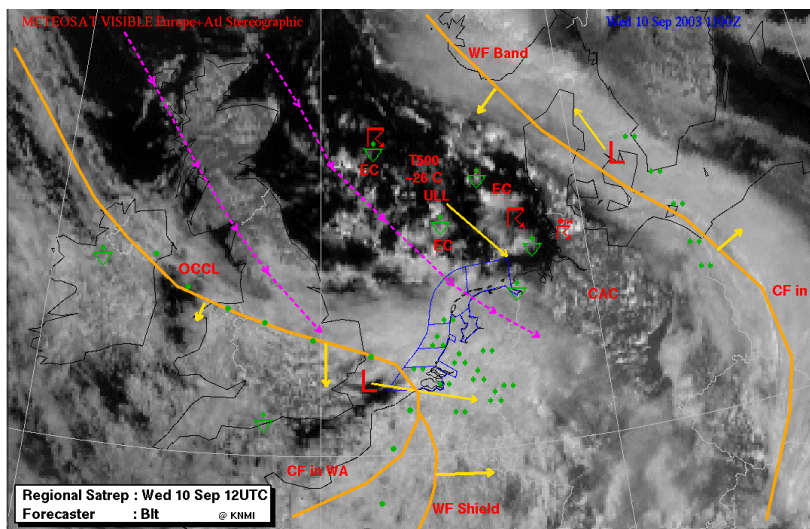


Figure 5.2 Regional SATREP picture September 10th 2003, 12 UTC. Source: KNMI

At 12 UTC and 18 UTC (not shown here) the frontal system is turning counter clockwise and this turning causes the (old) frontal system above Denmark to recede. This is probably causing warm advection. The low pressure area above Belgium is moving eastward. Behind the low pressure area wind direction is veering to north-west to north, causing cool polar air to approach the Netherlands.

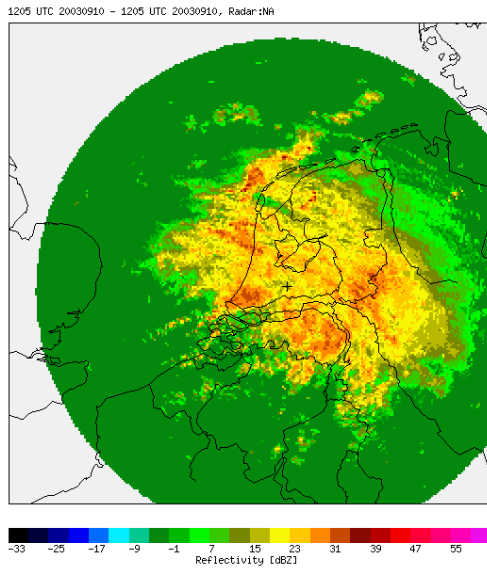


Figure 5.3 Radar image September 10th, 12 UTC,
Source: KNMI

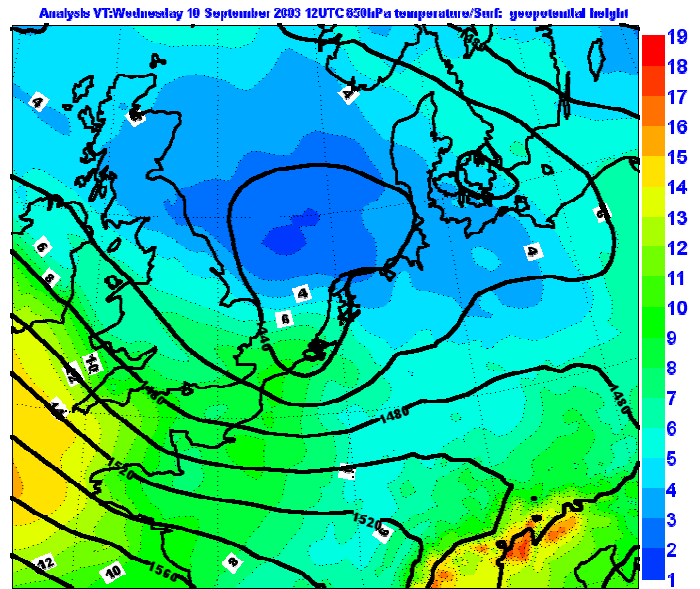


Figure 5.4 Analysis at 850 hPa, with height field and temperature. It can clearly be seen that warm air advection is taking place where the cold front in warm advection (CF in WA) is positioned in Figure 5.2. Source: Hirlam, KNMI

5.2.2 Calculated temperature advection

Before we examine the calculated advection from the Doppler radar wind profiles, let us first examine the wind profiles themselves (Figure 5.5).

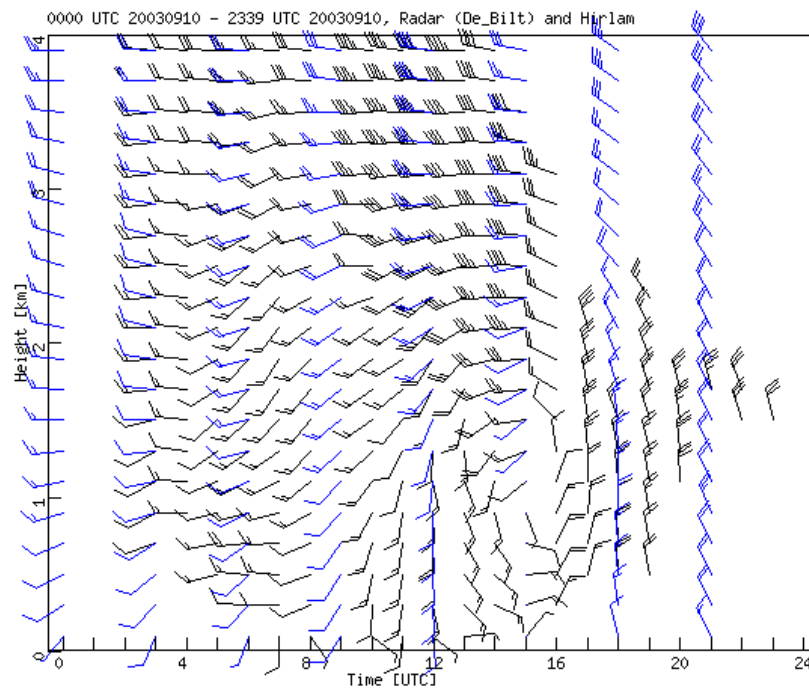


Figure 5.5 Wind profiles as observed by the Doppler radar in De Bilt, 10 September 2003. The Radar winds are given by the black barbs and the Hirlam winds by the blue barbs.

At 6 UTC we observe a westerly flow, backing to a southerly flow at 12 UTC. This is caused by the approaching of the low pressure area. We clearly observe the passage of the low pressure area around 14 UTC. We also notice that at 12 UTC, veering of the wind with height is taking place near the surface. However, higher in the atmosphere (> 3 km), this is not obvious. The profile of calculated temperature advection above De Bilt (Figure 5.9) shows however, that there is still considerable warm advection taking place above 3km.

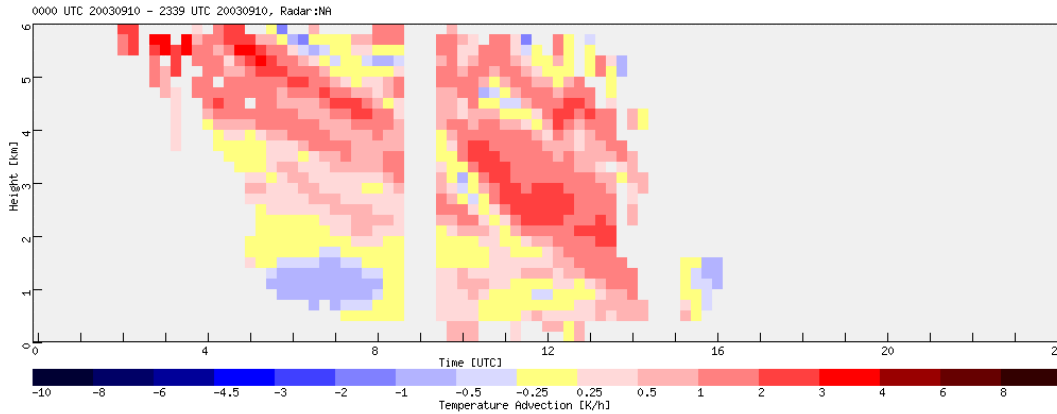


Figure 5.6 Temperature advection calculated from Doppler radar wind data on September 10th, 2003. The grey area indicates that no data were available

The cold air advection preceding the warm air advection at low levels (around 6 UTC, see Figure 5.6) indicates that the cold air advection caused by the upper air trough is moving slower than the frontal system, which is closing in. It clearly shows that the frontal zone is leaning forward. After 8 UTC, only warm air advection (WAV) is observed throughout the profile. Around 12 UTC most WAV is observed around 3 km, which agrees with the middle level at which most precipitation is often formed. This maximum of WAV leads to most ascending motions contributing to condensation.

5.2.3 Comparison radar-advection with Hirlam advection

In this section we will compare the calculated temperature advection from the Doppler radar with the calculated advection using Hirlam data. Advection is calculated using temperature gradients deduced from both the wind profiles (the “vertical method”) and the horizontal distribution of temperature (the “horizontal method”). See Chapter 3 for more information.

We will first compare the wind profiles of the radar and Hirlam, after which we will examine the temperature advection.

wind

The observed wind shows reasonable similarity to the wind calculated by Hirlam (Figure 5.7). The main difference is that the Hirlam wind profiles are a lot smoother: radar winds show more structure

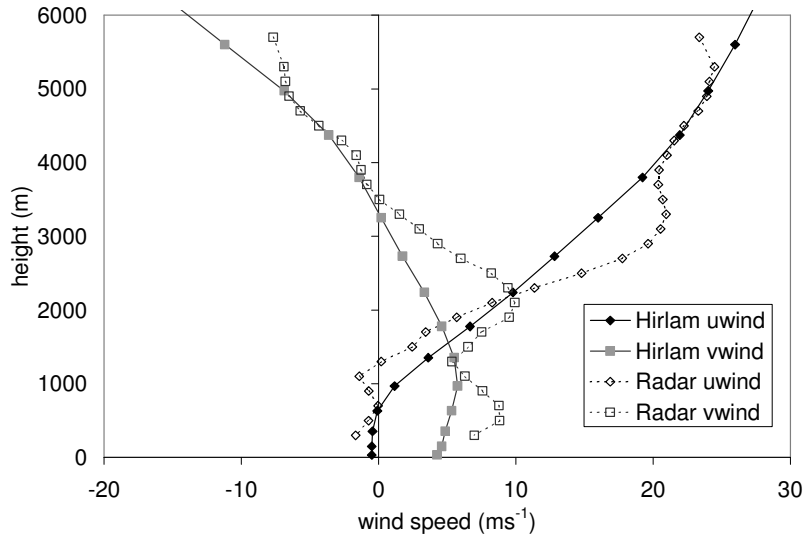


Figure 5.7 Wind velocity observed by the Doppler radar and calculated by Hirlam

Temperature advection

As was mentioned before, three different horizontal temperature advectons have been calculated (see for more information Chapter 3):

- 1) radar advection
- 2) Hirlam advection derived from wind profiles (referred to as “vertical” advection)
- 3) Hirlam advection derived from horizontal temperature distribution (referred to as “horizontal” advection)

In this section we will compare the profiles of these three advectons.

The three different methods all give positive temperature advection throughout the profile.

Up till 1 km the Hirlam advection using the “horizontal” and “vertical” method agree very well (Figure 5.8). After this, they diverge. This could imply that the assumptions for geostrophic wind and thermal wind are not valid here.

The radar advection shows much higher values than the Hirlam advection. This agrees with the differences in wind profiles we observed (Figure 5.7).

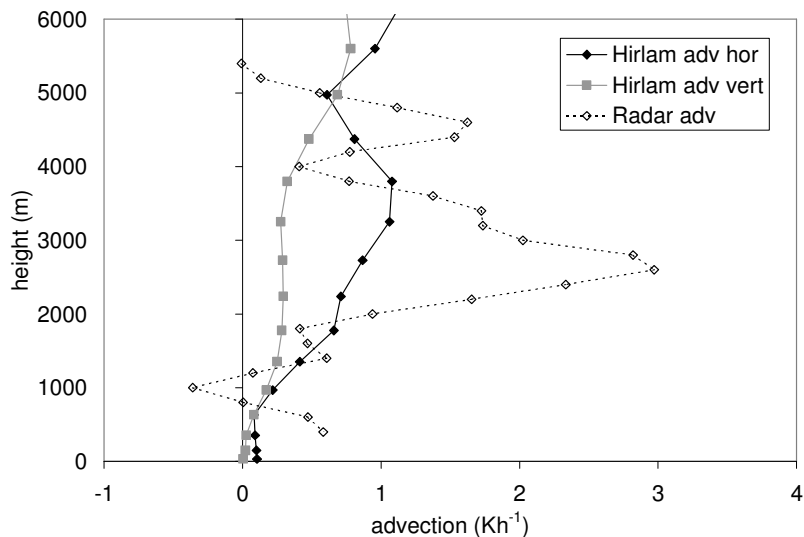


Figure 5.8 Advection calculated from Doppler radar wind profiles, Hirlam wind profiles (adv vert) and Hirlam temperature distribution (adv hor).

The cross section made over De Bilt (Figure 5.9, De Bilt is positioned at approximately 52°N and 5°E) confirms what we already saw in Figure 5.8 in the advection calculated from Hirlam data with the horizontal method. There is positive temperature advection throughout the layer. A maximum is found between 3 and 4 km and a small minimum around 5 km. This confirms that our approximation used when calculating the advection from horizontal temperature data from Hirlam is quite accurate. Because we made the cross section following the moving direction of the frontal system (from west to east), we can compare this cross section with position with our vertical cross section with time (Figure 5.6).

One feature that we would like to mention is the little patch of negative temperature advection preceding the profile of 12 UTC at De Bilt and located at 52.0° and 6.0° at 12 UTC, which we also found in Figure 5.6.

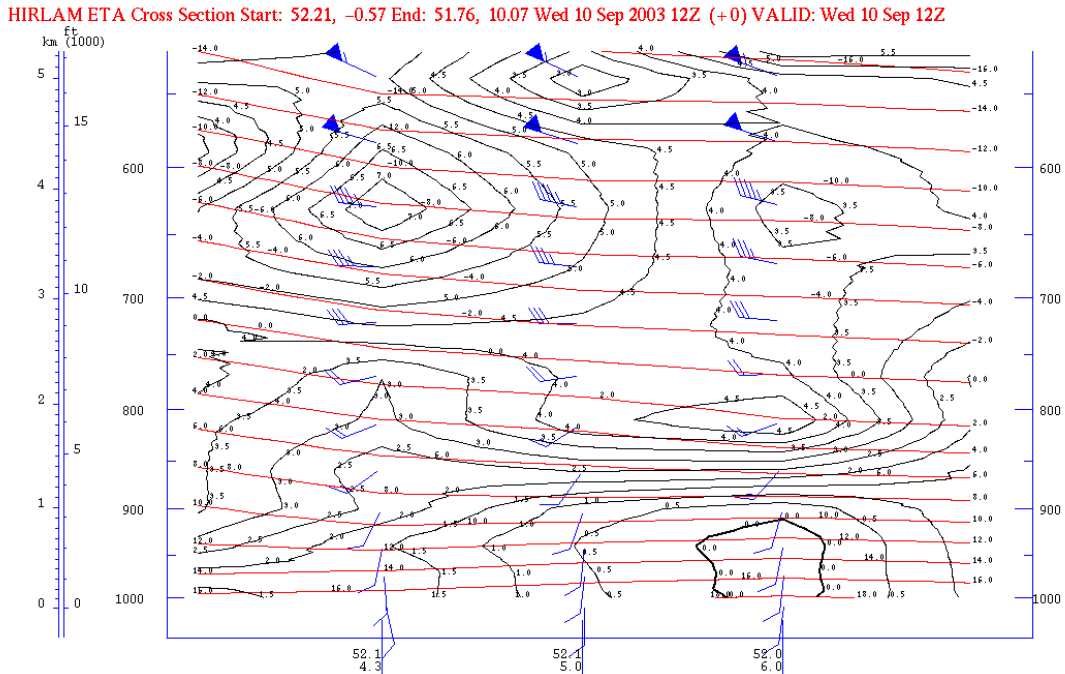


Figure 5.9 Vertical cross section of Hirlam analysis data (September 10th, 2003, 12 UTC) of temperature (red line, in °C), temperature advection (black line, in K/6h) and wind (blue barbs). The cross section is made on the line shown in Figure 5.10 and zoomed in around De Bilt (approx. 52°N and 5°E).

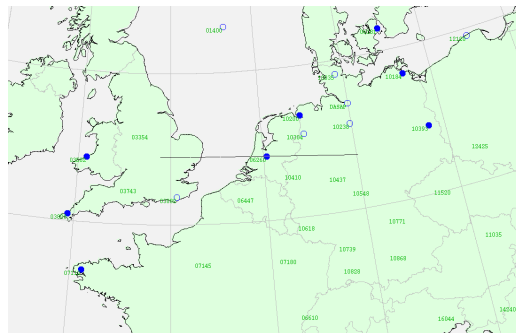


Figure 5.10 The cross section line belonging to cross-section in Figure 5.9

5.3 May 5th 2003, 6 UTC

5.3.1 Synoptic situation:

We will describe the synoptic situation using only the surface analysis of Hirlam. No SATREP pictures were available. However, we did use the guidance report accompanying the SATREP pictures.

On May 5th, 6 UTC a cold front is approaching the Netherlands from the west (Figure 5.11). It is preceded by a line of convergence causing most showers (see Figure 5.12) Despite the fact that the cold front is not very active, it is drawn for consistency with previous analyses (not shown). It is mentioned that the cold front is positioned in the middle of the gradient of potential temperature, which is not normally the case. With the SATREP method (not shown), the line preceding the cold front in Figure 5.11 is indicated as a warm conveyor belt preceding the cold front.

Analysis of this situation is difficult, proven by the differences between the analyses made by KNMI and that of the Met. Office. The Met. Office characterizes the active, rain producing line as the cold front, and has a “old cold front” to the west of that.

Because of the cold air above south of Ireland moving south, the upper airflow is backing, causing the system to move very slowly to the east and causing waves to originate in the frontal zone. Only in the beginning of the next day, the front reaches the border with Germany.

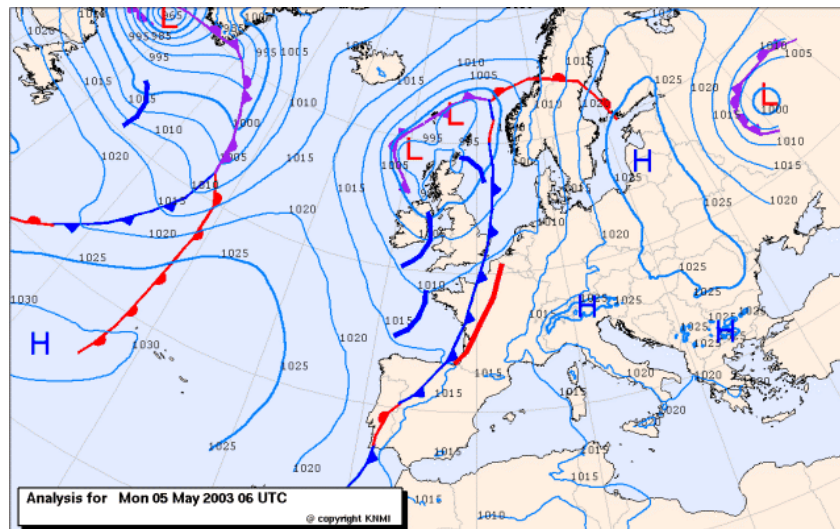


Figure 5.11 Synoptic situation on May 5th, 6 UTC. Source: KNMI

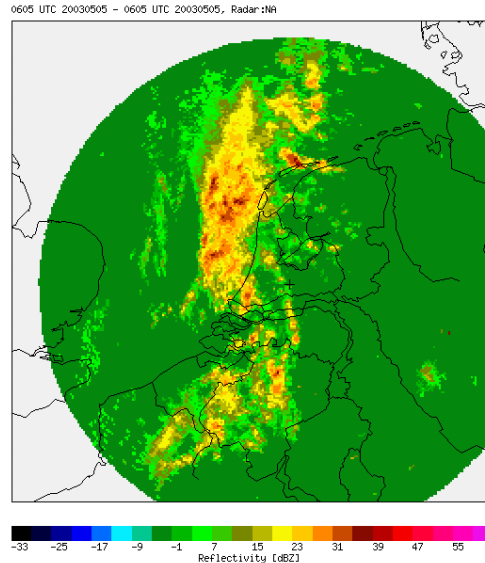


Figure 5.12 Radar image September 10th, 12 UTC, Source: KNMI

5.3.2 Calculated temperature advection

Figure 5.13 shows that at 6 UTC warm air advection is taking place below 3 km, while above cold air advection is found. This can be explained by the cold front (with cold advection) arching backward: near the surface cold advection is found, while above warm advection is taking place. Because the front is moving so slowly, the cold advection does not really penetrate the heights above 3.5 km, something that normally would occur if the front was moving faster.

The little patch of warm advection appearing between 1 and 2 km height around 10 UTC might indicate the passage of a wave in the cold front moving backwards (to the west). A similar area of WAV at lower levels is found the day after (not shown).

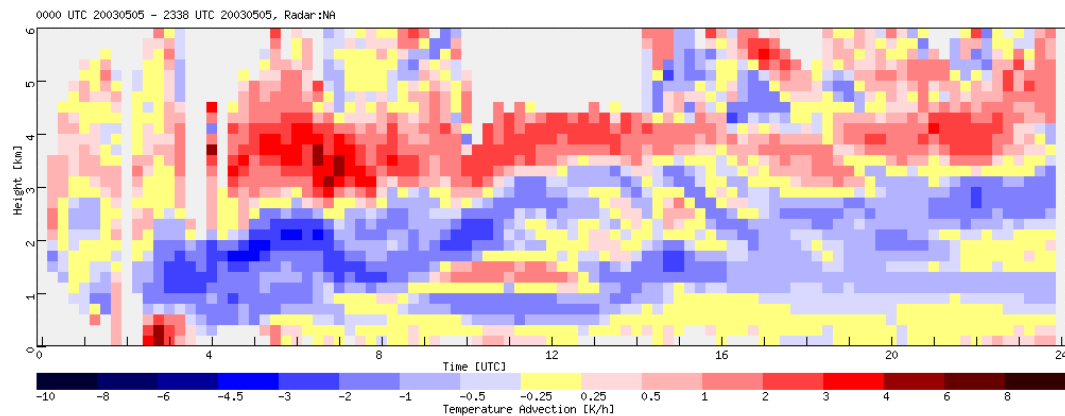


Figure 5.13 Temperature advection calculated from Doppler radar wind data on May 5th, 2003. The grey area indicates that no data were available

Because we found WAV overlying CAV during this case, we were interested whether we would also find this signal when examining radiosondes. With radiosondes, profiles of temperature are measured every 12 hours. Based on Figure 5.13, we would expect cooling below, and warming above 3 km between 0 and 12 UTC. Figure 5.14 shows us however, that cooling is taking place throughout the layer of 6 km, with the strongest cooling close to the surface. Apparently, at higher heights other terms in equation 3.18 counteract the influence of temperature advection.

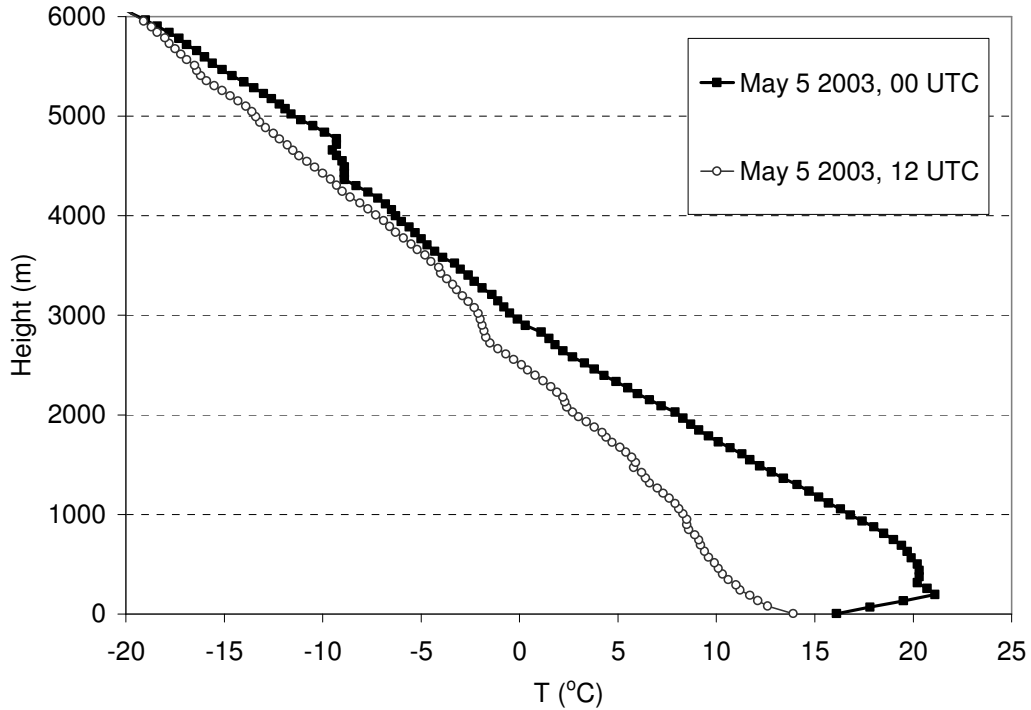


Figure 5.14. Temperature profiles measured by radiosonde

5.3.3 Comparison radar-advection with Hirlam advection

Overall, the profiles observed by the Doppler radar show much resemblance to those calculated by Hirlam (Figure 5.15). The main difference is that the radar profiles show more structure and more extreme values. Greatest differences are found in the u -wind.

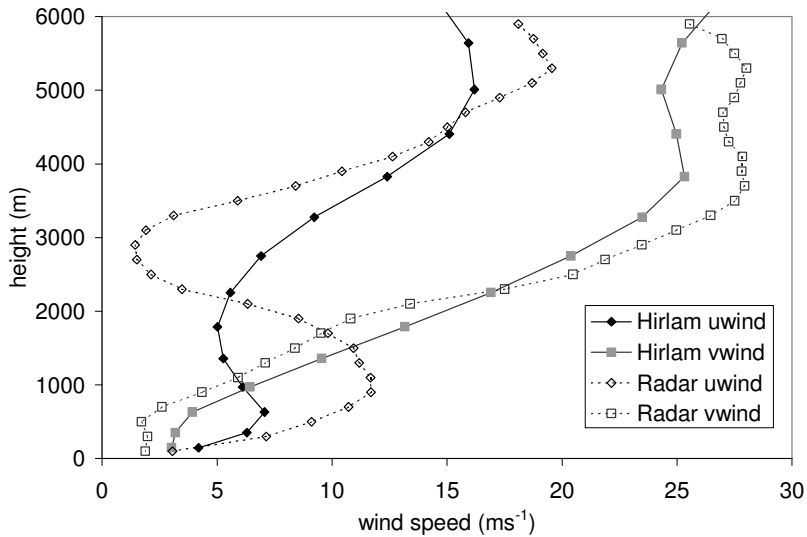


Figure 5.15 Wind velocity observed by the Doppler radar and calculated by Hirlam

Temperature advection

When comparing the advection calculated using the three different methods (see Chapter 3 for explanation on the methods used), we notice that they agree very well when it comes to the sign of the advection: they all give warm advection above cold advection. The two Hirlam advections show more

resemblance than in the previous case. Close to the surface the vertical method gives more warm advection than the horizontal case. This may be caused by friction (see section 5.1). The advection calculated using the Doppler radar wind profile, shows greater values (both positive and negative) than both advectations calculated using Hirlam data. This agrees with the differences we observed in wind profiles in Figure 5.15, where we observed more extreme values in the Doppler radar wind profile.

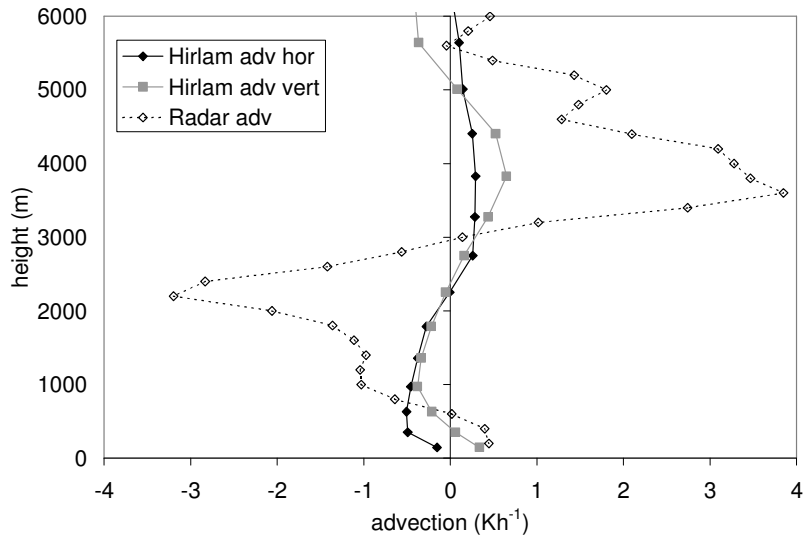


Figure 5.16 Advection calculated from Doppler radar wind profiles, Hirlam wind profiles (adv vert) and Hirlam temperature distribution (adv hor)

Figure 5.17 shows a cross section of temperature, temperature advection and wind with height zoomed in on the line shown in Figure 5.18. We observe again cold advection overlying warm advection around De Bilt.

Upper air currents indicate that the frontal system is moving in the direction shown in Figure 5.18 (i.e. it is moving toward the NNE). This also explains why the system takes so long to leave the country. It can be concluded from Figure 5.17 that after 6 UTC, an area of cold advection might cross De Bilt (indicated by the area of CAV in the upper left corner of Figure 5.17). This might correspond to the patch of cold advection observed by the Doppler radar (Figure 5.15) between 15 and 17 UTC just above 4 km, although this is higher than the heights indicated in Figure 5.17.

HIRLAM ETA Cross Section Start: 44.00, 0.00 End: 57.61, 10.49 Mon 05 May 2003 06Z (+0) VALID: Mon 05 May 06Z

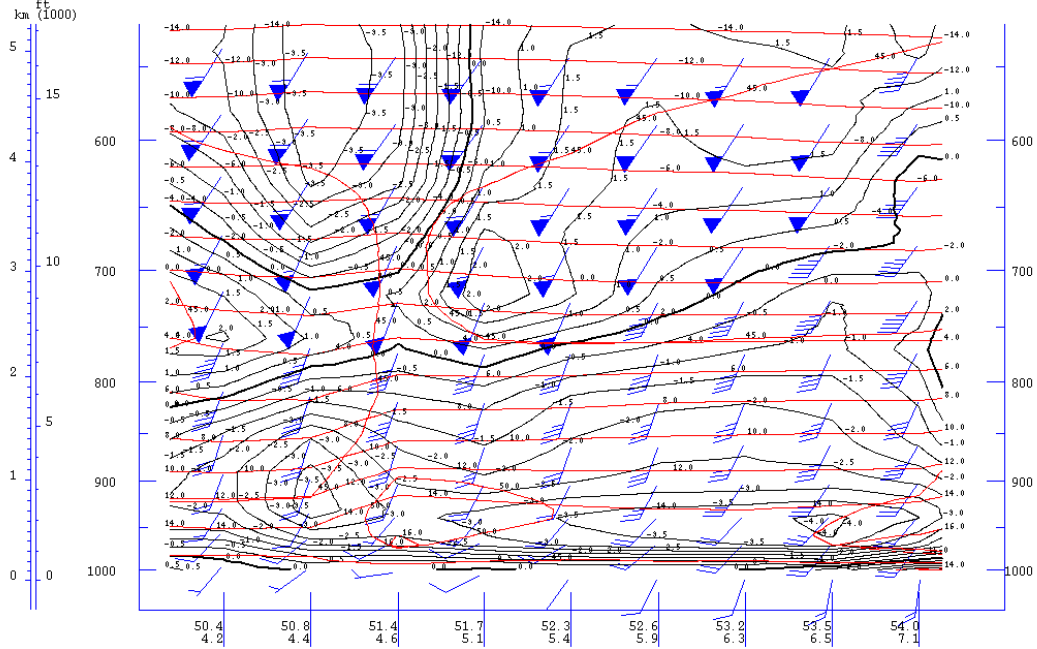


Figure 5.17 Vertical cross section of Hirlam analysis data (May 5th 2003, 6 UTC) of temperature (red line, in °C), temperature advection (black line, in K/6h) and wind (blue barbs). The cross section is made on the line shown in Figure 5.19 and zoomed in around De Bilt (approx. 52°N and 5°E).

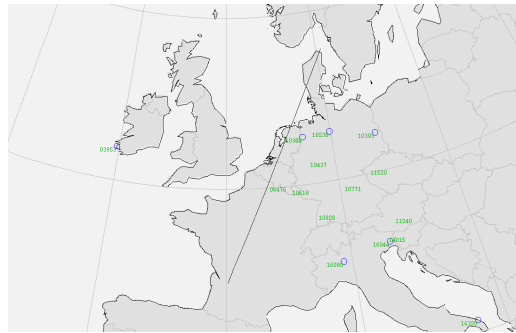


Figure 5.18 The cross section line belonging to cross-section in Figure 5.17

Chapter 6 Conclusions and recommendations

Wind profiles measurements performed with the Doppler radar at De Bilt, The Netherlands, have been used to study the temperature advection deduced from the thermal wind. For two cases, May 5th 2003, 6 UTC and September 10th 2003, 12 UTC the profiles of advection up to 6 km have been compared to advection calculated from Hirlam output. We approximated the advection from Hirlam in two different ways: 1) with the thermal wind and 2) using an estimate for the temperature gradients using values for T at a small grid centred around De Bilt.

6.1 Conclusions

As a result of this pilot study a few conclusions can be drawn:

- Figures showing the advection calculated from Doppler radar wind profiles show consistent patterns. The features can be explained by the synoptic situation.
- Advection calculated from Doppler radar wind profiles show more extreme values than the advection calculated from Hirlam data.
- Displaying calculated temperature advection like we did in this report emphasizes the rotation in the wind field, which would go unnoticed when examining just the wind profiles.
- Use of the calculated advection depends on the extent of geostrophy of the synoptic situation. This method is probably not useful in mesoscale phenomena. The calculated advection might serve as a first estimation of the tendency in temperature taking place in the atmosphere.
- Especially nowcasting might benefit from usage of Doppler radar temperature advection profiles, provided that knowledge about interpretation of the images increases.

6.2 Recommendations

- Analyze more cases to get a better estimate of the importance of the assumption of geostrophy. The Rossby number can be calculated to estimate whether the geostrophic approximation is valid.
- Make figures of the calculated advection deduced from Doppler radar wind profiles available for weather forecasters, for example by a real time display on the Intranet. This should be accompanied by an effort to increase knowledge on how the observed temperature advection can be interpreted and used for nowcasting.

Acknowledgements

I would like to thank Iwan Holleman for giving me the opportunity to do my internship at the KNMI. Iwan, thank you for your enthusiasm and your guidance and support during this research. Siebren de Haan is acknowledged for his help on C programming. I appreciate very much the effort and time Sander Tijm invested in helping me with everything concerning Hirlam data. Han Mellink is acknowledged for his help with the analyses of the synoptic situation during the cases, for making the figures using archive data and for the valuable discussions I had with him.

References

Bluestein, 1992: *Synoptic - dynamic meteorology in midlatitudes, Vol. 1: Principles of kinematics and dynamics*. Oxford University Press, New York, 431 p

Holleman, 2003: *Doppler radar wind profiles*. Scientific Report, WR-2003-02, KNMI, De Bilt, 73 pp.

Holleman and Beekhuis, 2003: Analysis and correction of dual PRF velocity data. *J. Atmos. Oceanic Technol.*, **20**, 443- 453.

Holton, 1979: *An introduction to dynamic meteorology*. Second edition, Academic press, New York 393 pp.

Stull, 2000: Second edition for meteorology for scientists and engineers, a technical companion book with Ahrens's Meteorology today. Brooks/Cole, Pacific Grove, 502 pp.

URL1 http://snowball.millersville.edu/~adecaria/ESCI343/esci343_lesson04_QG_tendency_eqn.html

URL2 <http://hdf.ncsa.uiuc.edu/index.html>

URL3 http://www.knmi.nl/onderzk/imageformat/bik_web/bik_hdf5/hdf5_intro.htm

Appendix A Symbols and constants

List of symbols

λ	wavelength	(m)
p	pressure	(Pa)
ρ	density	(kg/m ³)
ϕ	latitude	(rad)
φ	phase shift	(-)
Φ	geopotential	(m ² s ⁻²)
f	Coriolis parameter	(s ⁻¹)
H	geopotential height	(m)
p	pressure	(Pa)
Q	heat	(Jkg ⁻¹)
R	gas constant for dry air	(JK ⁻¹ kg ⁻¹ or kPam ³ K ⁻¹ kg ⁻¹)
σ	a measure of static stability	(m ³ kg ⁻¹ Pa ⁻¹)
t	time	(s)
T	temperature	(K)
u	x- component of velocity (eastward)	(ms ⁻¹)
u_g	x- component of the geostrophic wind (eastward)	(ms ⁻¹)
u_T	x- component of the thermal wind (eastward)	(ms ⁻¹)
v	y- component of velocity (northward)	(ms ⁻¹)
v_g	y- component of the geostrophic wind (northward)	(ms ⁻¹)
v_T	y- component of thermal wind (northward)	(ms ⁻¹)
x,y,z	Eastward, northward and upward distance, respectively	
ω	vertical velocity in pressure coordinates	(Pas ⁻¹)
z	height	(m)

List of constants

C_p	specific heat at constant pressure	= 1005	(Jkg ⁻¹ K ⁻¹)
g	gravitational acceleration	≈ 9.81	(ms ⁻²)
g_0	global average of gravity at mean sea level	= 9.80665	(ms ⁻²)
R	Gas constant for dry air	= 287.053	(Pa m ³ K ⁻¹ kg ⁻¹)
Ω	Angular speed of rotation of the earth	= 7.292 · 10 ⁻⁵	(rad s ⁻¹)

Appendix B Influence of grid size on the calculated temperature gradient

In section 3.3 we mentioned that the grid size that was taken around The Bilt to calculate the temperature gradient did not influence the calculated advection to a great extent.

A small sensitivity analysis was performed for the case of May 5th 2003, 6 UTC. The temperature advection was calculated using temperature values interpolated to 5 different grid sizes: 0.25, 0.5, 1, 2, and 4 degrees for Δx and Δy in Figure B.1 (same as Figure 3.5)

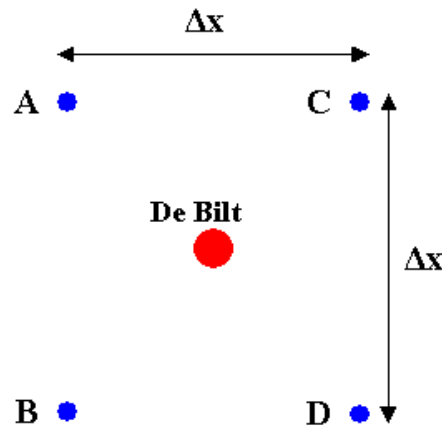


Figure B.1 Grid around De Bilt used for advection calculation from Hirlam data using the “horizontal method”

Figure B.2 shows that the grid size influences the calculated advection to a small degree only. Only when the grid size is enlarged to 4 degrees, we get a very different outcome for the advection. For our analyses, we used a 1 x 1 grid.

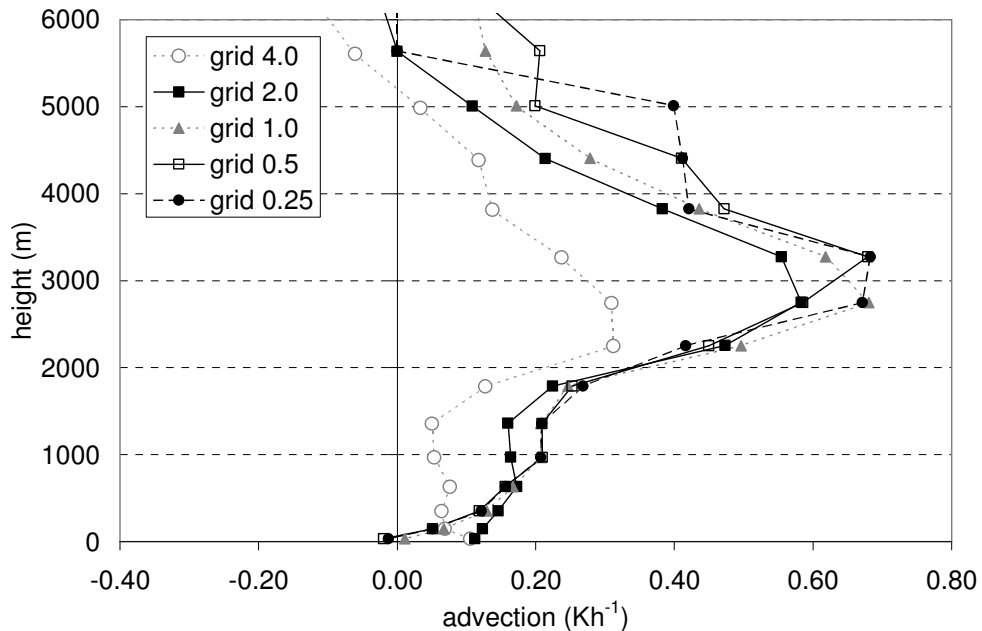


Figure B.2 Advection calculated from Hirlam temperature distribution using 5 different grid sizes.

Appendix C Program code used for advection calculation

C.1 Calculating temperature advection from Doppler radar wind profiles.

Input files are the VP2 files created from processing Doppler radar data. There are different ways to calculate the temperature advection from Doppler radar data:

- 1) One file at the time:
 - use C-code “thermalwind”. Usage:
`thermalwind <inputfile.h5> <outputfile.h5>`
 - for plotting use:
`image2plot outputfile.h5 -Ofigure.png -fldX -size1000`
 - look at figures: `xv figure.png`
- 2) Many files at once:
 - Use script “advection”. This script uses C-program “thermalwind” to calculate temperature advection. Usage:
`advection *.h5`. (Names for the output HDF5 files will be created by the script by changing VP2 into ADV)
 - to look at all figures at once use script “alleszien”. This script calls `xv` to view figures. Usage: `alleszien *.png`
- 3) One file at the time with many output files:
 - use C-code “thermalwind_debug”. Usage:
`thermalwind_debug <inputfile.h5> <outputfile.h5>`
Next to the output HDF5 file, output files will be generated (in .txt files) for unscaled u and v wind, scaled u and v wind, filtered u and v wind (using standard deviation data), thermal winds u_T and v_T , temperature gradients in both x and y direction, temperature advection in x and y direction, total temperature advection.

NB. The “thermalwind” code creates a HDF5 file in which the “imageN/image_product_name” hasn’t been changed yet from e.g. RAD_NL50_VP2_24H_200305050000.h5 to RAD_NL50_ADV_24H_200305050000.h5

C.2 Calculating temperature advection from Hirlam data

Input files are interpolated Hirlamfiles. Input tar. files are copied from /net/bgomos/fa/mw/2003/LAMH_OPR/. Contents of the .tar files can be viewed using `tar tvf tarfile.tar`. A single file can be taken out of the .tar files using `tar xvf tarfile.tar subfile`

Subfiles have names like LAMH_LFM_200305050600_00000_AB. These files are interpolated to a grid around De Bilt using `intparea3` (interpolate area). This script uses `intp506.x` for interpolation (from bin directory). One of the outputfiles is a text file like LAMH_LFM_200305050600_00000_ABi.txt, which serves as input file for the advection calculation.

Both “horizontal” and “vertical” temperature advection (see Chapter 3 for explanation) is calculated using C-code “hirlamadv”.

Usage: `hirlamadv <inputfile.txt.>`

Output file is “Hirlamoutput.txt”, with a header indicating the meaning of the different columns.